

## Rode's iterative calculation of surface optical phonon scattering limited electron mobility in N-polar GaN devices

Krishnendu Ghosh and Uttam Singiseti

Citation: [Journal of Applied Physics](#) **117**, 065703 (2015); doi: 10.1063/1.4907800

View online: <http://dx.doi.org/10.1063/1.4907800>

View Table of Contents: <http://scitation.aip.org/content/aip/journal/jap/117/6?ver=pdfcov>

Published by the [AIP Publishing](#)

---

### Articles you may be interested in

[Interface roughness scattering in ultra-thin N-polar GaN quantum well channels](#)

Appl. Phys. Lett. **101**, 012101 (2012); 10.1063/1.4732795

[Polar-optical-phonon-limited electron mobility in GaN/AlGaIn heterojunctions](#)

AIP Conf. Proc. **1447**, 947 (2012); 10.1063/1.4710316

[Influence of AlN interlayer on the anisotropic electron mobility and the device characteristics of N-polar AlGaIn/GaN metal-insulator-semiconductor-high electron mobility transistors grown on vicinal substrates](#)

J. Appl. Phys. **108**, 074502 (2010); 10.1063/1.3488641

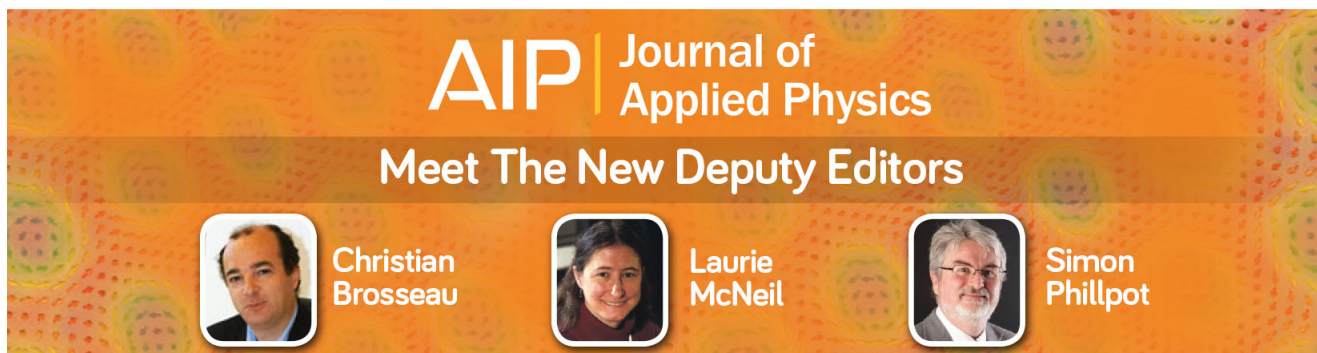
[Improved two-dimensional electron gas transport characteristics in AlGaIn/GaN metal-insulator-semiconductor high electron mobility transistor with atomic layer-deposited Al<sub>2</sub>O<sub>3</sub> as gate insulator](#)

Appl. Phys. Lett. **95**, 223501 (2009); 10.1063/1.3268474

[Analysis of dislocation scattering on electron mobility in GaN high electron mobility transistors](#)

J. Appl. Phys. **93**, 10046 (2003); 10.1063/1.1577406

---

A promotional banner for the Journal of Applied Physics. It features the AIP logo and the journal title at the top. Below that, the text 'Meet The New Deputy Editors' is displayed. Three circular headshots of the new deputy editors are shown, each with their name written below it: Christian Brosseau, Laurie McNeil, and Simon Phillpot. The background is a dark orange with a pattern of colorful, abstract shapes.

# Rode's iterative calculation of surface optical phonon scattering limited electron mobility in N-polar GaN devices

Krishnendu Ghosh<sup>a)</sup> and Uttam Singiseti<sup>b)</sup>

*Electrical Engineering Department, University at Buffalo, Buffalo, New York 14260, USA*

(Received 20 October 2014; accepted 28 January 2015; published online 10 February 2015)

N-polar GaN channel mobility is important for high frequency device applications. Here, we report theoretical calculations on the surface optical (SO) phonon scattering rate of two-dimensional electron gas (2DEG) in N-polar GaN quantum well channels with high-k dielectrics. Rode's iterative calculation is used to predict the scattering rate and mobility. Coupling of the GaN plasmon modes with the SO modes is taken into account and dynamic screening is employed under linear polarization response. The effect of SO phonons on 2DEG mobility was found to be small at  $>5$  nm channel thickness. However, the SO mobility in 3 nm N-polar GaN channels with  $\text{HfO}_2$  and  $\text{ZrO}_2$  high-k dielectrics is low and limits the total mobility. The SO scattering for  $\text{SiN}$  dielectric on GaN was found to be negligible due to its high SO phonon energy. Using  $\text{Al}_2\text{O}_3$ , the SO phonon scattering does not affect mobility significantly only except the case when the channel is too thin with a low 2DEG density. © 2015 AIP Publishing LLC. [<http://dx.doi.org/10.1063/1.4907800>]

## I. INTRODUCTION

The key advantage of the GaN devices is the high two-dimensional electron gas (2DEG) mobility ( $\sim 2000 \text{ cm}^2/\text{V.s}$ ) in combination with wide bandgap that enables both high frequency and high breakdown operation.<sup>1</sup> Understanding the limiting mechanisms of the 2DEG mobility<sup>2-7</sup> is critical as novel GaN device structures are explored.<sup>8-11</sup> In recent years, there has been considerable interest and progress in the N-polar GaN field-effect transistors (FET) for ultra high frequency and high breakdown applications because of the presence of back barrier for electron confinement.<sup>12-15</sup> In the ultra-thin-body silicon-on-insulator (UTB-SOI) like N-polar GaN devices, the quantum well channel thickness is critical to scaling of these devices to ultra-small gate lengths.<sup>14,16</sup> In addition, the equivalent oxide thickness (EOT) of the gate barrier also needs to be scaled in these devices by decreasing the thickness and also by incorporating high-k dielectrics.

However, both the channel thickness scaling<sup>17,18</sup> and gate barrier scaling have been shown to affect the 2DEG mobility. The channel thickness has also been shown experimentally to affect the channel velocity in devices.<sup>16</sup> Incorporation of high-k gate dielectrics deposited by atomic layer deposition (ALD) has been reported to affect the channel transport properties in GaN devices.<sup>4,6</sup> Through optimization of device structure and growth conditions, high conductivity 5 nm N-polar GaN channel devices with high mobilities ( $1100 \text{ cm}^2/\text{V.s}$ ) have been recently reported.<sup>19-22</sup> In order to continue further increase in the high frequency performance in sub-20-nm gate length devices, extreme channel thickness scaling ( $<5$  nm) with high 2DEG mobility will be necessary. It is therefore important to evaluate the

limits of 2DEG mobility arising from high-k dielectrics on these thin channels.

The deposition of high-k dielectrics on GaN results in additional scattering mechanisms that include remote interfacial charge scattering<sup>4,6</sup> and remote roughness scattering.<sup>2</sup> Another important scattering mechanism originating from high-k dielectrics is the surface/interfacial polar optical phonon scattering, which has not been considered previously in N-polar GaN devices.

Surface optical (SO) phonon scattering of the 2DEG at the interface between polar silicon dioxide and Si channel in a Si MOSFET was reported by Hess<sup>23</sup> and Ferry.<sup>24</sup> The SO phonon is also referred to as remote interface phonon (RIP) and surface polar phonon (SPP) in the literature. The SO scattering was found to be a critical mobility limiting mechanism in Si MOSFETs with high-k dielectrics<sup>25</sup> and for III-V MOSFETs<sup>26</sup> with high-k. In recent years, SO phonon scattering has been reported as the limiting mechanism for room temperature mobility of graphene.<sup>27-30</sup> Here, we report the impact of surface optical phonon (SOP) scattering on the mobility of N-polar channel devices. We also report on the dependence of the SO phonon scattering rate on the thickness of the N-polar GaN channel.

Because of its simplicity, the relaxation time approximation (RTA) is widely used to calculate mobility in semiconductors. However, since SO phonon scattering is inelastic, RTA method cannot be used. A full solution of Boltzmann transport equation (BTE) is complex and time consuming. Here, we use Rode's iterative technique to calculate the SO phonon scattering rate and mobility.<sup>31,32</sup> We also incorporate full dynamic screening including plasmon contribution to improve the accuracy of the calculations. In Sec. II, we discuss SO phonon dispersion in high-k/GaN heterostructures, and in Sec. III, we describe the Rode's iterative technique for 2DEG mobility.

<sup>a)</sup>Email: kghosh3@buffalo.edu

<sup>b)</sup>Email: uttamsin@buffalo.edu, Tel.: 716-645-1536, Fax: 716-645-3656

## II. SURFACE EXCITATION MODES IN METAL/HIGH- $\kappa$ /GaN/AlN/GaN SYSTEM

Surface or interface optical phonon modes exist at the intersection of two materials if one of them is a polar material.<sup>33,34</sup> These modes are confined to the interface and decay exponentially from it. In the case of high- $k$  dielectric on semiconductor, the polar or ionic nature of the high- $k$  leads to surface/interface phonon modes. The interface modes arise due to the electrostatic boundary condition imposed on the phonon electric field.<sup>35</sup> Each transverse optical (TO) mode in the high- $k$  gives rise to a SO mode at the interface. On the other hand, the 2DEG in the substrate gives rise to collective plasma oscillation which can couple with the decaying surface modes. This coupling (also called hybridization) has significant effect on the interaction of an individual electron with the surface modes.<sup>36</sup>

### A. Screened plasmon coupled surface modes

In order to calculate the SO phonon frequency, first we consider unscreened surface modes for the metal-high- $k$ -N-polar GaN system.<sup>25–27</sup> Fig. 1 shows the co-ordinate system used for the SO phonon dispersion calculation. The high- $k$ /GaN interface is at  $z=0$ , the high- $k$  oxide of thickness  $t_{ox}$  and GaN channel of thickness ( $t_{ch}$ ) are in the negative and positive half planes, respectively. The structure also includes a bottom AlN barrier layer. To calculate the dispersion of interface phonon modes, exponentially decaying phonon mode potential is assumed as given in the equation below

$$\phi_{q,\omega}(z) = \begin{cases} 0 & -t_{ox} \leq z < \infty \\ b_{q,\omega} \cosh q(z + t_{ox}) & -t_{ox} \leq z \leq 0 \\ c_{q,\omega} \exp(qz) + d_{q,\omega} \exp(-qz) & 0 \leq z \leq t_{ch} \\ f_{q,\omega} \exp(qz) + g_{q,\omega} \exp(-qz) & t_{ch} \leq z \leq t_{ch} + t_{AlN} \\ h_{q,\omega} \exp(-qz) & z \geq t_{ch} + t_{AlN}. \end{cases} \quad (1)$$

Equation (1) shows the unscreened potential due to the surface modes. But, the actual potential seen by an electron in the channel is screened collectively by the 2DEG. To obtain expression for a screened potential, we use a Green's function based formalism as was used in case of graphene in Ref. 36. However, unlike graphene, 2DEG here is a quasi-2D system, and hence, the behavior of the screened potential is different from that in graphene. From linear response theory, the screened potential is given by<sup>36</sup>

$$\phi_{q,\omega}^{scr}(z) = \phi_{q,\omega}(z) + e^2 \int dz' G_q(z, z') \chi(q, \omega) f(z') \phi_{q,\omega}^{scr}(z'), \quad (2)$$

where the Green's function obeys the equation of motion,

$$\left( \frac{\delta^2}{\delta z^2} - q^2 \right) G_q(z, z') = \frac{1}{(\epsilon_{GaN}^0)} \delta(z - z'), \quad (3)$$

$\chi(q, \omega) = m^*/\pi \cdot \hbar^2$  is the polarizability of the 2DEG,<sup>37</sup> and  $f(z')$  is the spatial distribution of the 2DEG. The solution of Eq. (3) is of the form given in Eq. (4). The coefficients in the equations are obtained by applying Dirichlet and Neumann boundary conditions (Appendix A) at different

$$G_q(z, z') = -\frac{1}{2q\epsilon_{GaN}^0} \begin{cases} \alpha_q [\exp(q(z - z')) + \exp(-q(z + z' + 2t_{ox}))] & -t_{ox} \leq z < 0 \\ \beta_q \exp(-q|z - z'|) + \gamma_q \exp(-q(z + z')) + \eta_q \exp(q(z + z')) & 0 \leq z < t_{ch} \\ \kappa_q \exp(-q(z - z')) + \lambda_q \exp(q(z + z')) & t_{ch} \leq z \leq t_{ch} + t_{AlN} \\ \zeta_q \exp(-q(z - z')) & z \geq t_{ch} + t_{AlN} \end{cases} \quad (4)$$

interfaces of the system (Fig. 1).

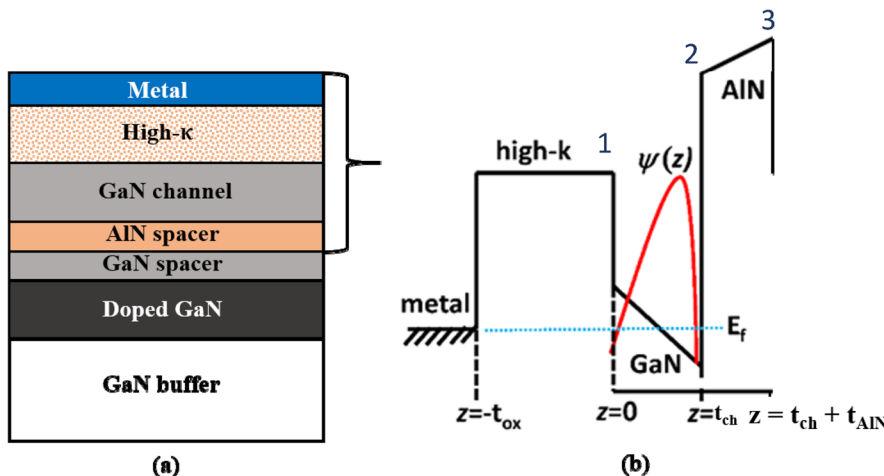


FIG. 1. (a) Schematic cross-section of the N-polar GaN device. The thicknesses of the high- $\kappa$ , AlN spacer, GaN spacer, and doped GaN layer are 5 nm, 2 nm, 5 nm, and 5 nm, respectively. The thickness of the GaN channel is varied for studying variation in mobility. The doping of the doped GaN layer is  $10^{13}/\text{cm}^2$ . (b) Schematic conduction band profile of the device. The figure shows the  $z$ -co-ordinate used for the calculations. Different interfaces are numbered as 1, 2, and 3 to help recognize the origin of different surface modes later in Fig. 2.

Using this form of the Green's function in Eq. (2),  $\phi_{q,\omega}^{scr}(z)$  can be obtained. Though a direct closed form expression is not obtained, a kernel ( $T$ ) can be calculated from Eq. (2) to estimate  $\phi_{q,\omega}^{scr}(z)$  from  $\phi_{q,\omega}(z)$ .

$$\{\Phi_{q,\omega}^{scr}\} = [T_{q,\omega}] \{\Phi_{q,\omega}\} \quad (5a)$$

$$[T_{q,\omega}] = [[\mathbf{I}] - \Delta z e^2 \chi(q, \omega) [\mathbf{G}_q] [f]]^{-1}. \quad (5b)$$

Here,  $\Delta z$  is the grid spacing used and  $[\mathbf{I}]$  is an identity matrix of size  $n \times n$ , where  $n$  is the number of grid points in real space.  $[\mathbf{G}_q]$  is the Green's function matrix, and  $[f]$  is the diagonal electron probability density matrix. The elements of the column vectors  $\{\Phi_{q,\omega}^{scr}\}$  and  $\{\Phi_{q,\omega}\}$  contain the screened and unscreened potentials at different spatial locations. Having obtained  $\{\Phi_{q,\omega}^{scr}\}$ , electrostatic boundary conditions are applied to obtain the dispersion relation. A perfect metal is used as a gate so that screened phonon field goes to zero at the metal. The channel dielectric response consists of both lattice and plasmon contribution. The dielectric responses are listed below

$$\begin{aligned} \epsilon_{ox}(\omega) &= \epsilon_{ox}^\infty + \frac{f_1 \omega_{TO1}^2}{\omega_{TO1}^2 - \omega^2} + \frac{f_2 \omega_{TO2}^2}{\omega_{TO2}^2 - \omega^2} \\ \epsilon_{GaN}(\omega) &= \epsilon_{GaN}^\infty + \frac{f_3 \omega_{TO3}^2}{\omega_{TO3}^2 - \omega^2} \\ \epsilon_{ch}(\omega) &= \epsilon_{GaN}^\infty + \frac{f_3 \omega_{TO3}^2}{\omega_{TO3}^2 - \omega^2} - \epsilon_{GaN}^\infty \frac{\omega_p^2}{\omega^2} \\ \epsilon_{AlN}(\omega) &= \epsilon_{AlN}^\infty + \frac{f_4 \omega_{TO4}^2}{\omega_{TO4}^2 - \omega^2}. \end{aligned} \quad (6)$$

Here,  $\omega_p$  is the plasmon frequency of the GaN 2DEG.<sup>37</sup> The coupling strengths are  $f_1 = \epsilon_{ox}^i - \epsilon_{ox}^0$ ,  $f_2 = \epsilon_{ox}^\infty - \epsilon_{ox}^i$ ,  $f_3 = \epsilon_{GaN}^\infty - \epsilon_{GaN}^0$ , and  $f_4 = \epsilon_{AlN}^\infty - \epsilon_{AlN}^0$ . The dielectric functions ( $\epsilon$ ) with superscripts of  $\infty$ ,  $i$ , and  $0$  correspond to high frequency, intermediate frequency, and DC dielectric constants. The oxide thickness is taken to be 5 nm in this study. The high-k dielectric function parameters were taken from Ref. 25, the SiN parameters were taken from Ref. 38 (see Table I). The dispersion of the interface modes is shown in Fig. 2 for metal-HfO<sub>2</sub>-GaN-AlN-GaN system.

As seen in the Fig. 2, there are nine modes present. These modes are all surface modes coupled with the 2DEG plasmon mode. In this figure, the lower two modes are originating from the TO1 and TO2 modes of the high-k. Plasmon coupling is not present for  $\omega_1$  due to the absence of energy overlap with the plasmon mode (dashed line in

TABLE I. Different TO phonon energies and dielectric function parameters for Al<sub>2</sub>O<sub>3</sub>, HfO<sub>2</sub>, and ZrO<sub>2</sub> are taken from Ref. 25, while those for SiN are taken from Ref. 38.

	Al <sub>2</sub> O <sub>3</sub>	HfO <sub>2</sub>	ZrO <sub>2</sub>	SiN
$\epsilon_0$	12.53	22.00	24.00	7.5
$\epsilon_{int}$	7.27	6.58	7.75	...
$\epsilon_\infty$	3.20	5.00	4.00	4.17
$\omega_{TO1}$ (meV)	48.00	12.48	17.00	103.00
$\omega_{TO2}$ (meV)	78.10	48.18	58.00	...

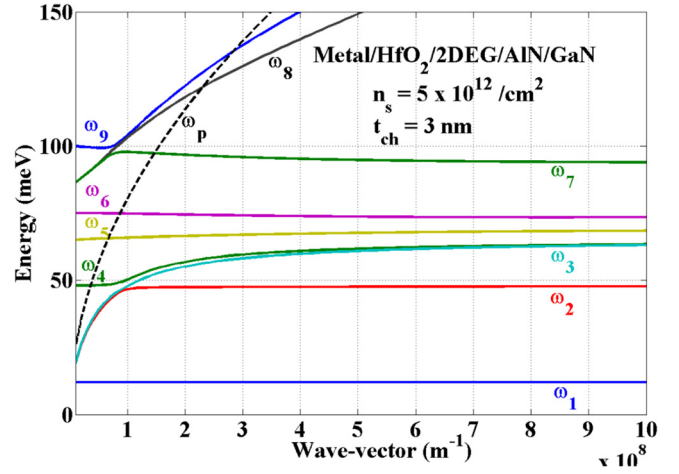


FIG. 2. Calculated dispersion of the plasmon coupled surface modes for metal-HfO<sub>2</sub>-2DEG-AlN-GaN system.  $\omega_1$ - $\omega_4$  denote the modes that arise at interface 1 of Fig. 1.  $\omega_7$ - $\omega_9$  arise from interface 2, while  $\omega_5$  and  $\omega_6$  arise from interface 3. The pure plasmon mode is shown by a black dotted line.

Fig. 2). Plasmon coupling is observed for TO2 mode ( $\omega_2$  in Fig. 2). The GaN plasmon couples to surface modes at interface 1 ( $\omega_1$ - $\omega_4$ ) and interface 2 ( $\omega_7$ - $\omega_9$ ) only, while the remote surface modes at interface 3 ( $\omega_5$  and  $\omega_6$ ) do not couple. For calculation of mobility, we need to consider the scattering interaction of an electron with the phonon content only since interaction with the plasmon is just exchange of momentum and energy among the electrons themselves without changing the mobility.<sup>36</sup> Next, we decouple the surface-phonon mode contribution from the coupled modes.

## B. Phonon contribution in coupled modes

We follow the approach given in Ref. 36 to separate out phonon contributions. Since, in our case the plasmon mode sees boundaries on both sides- high-k and AlN; we obtain two modes from the plasmon contribution. Here we calculate the contribution of the surface modes arising from the high-k TO phonons using the following equation:

$$\phi_{q,\omega}^{TO\vartheta,i} = \frac{\prod_{j=1}^8 (\omega_q^{(i)2} - \omega_q^{(j,-TO\nu)2})}{\prod_{j \neq i} (\omega_q^{(i)2} - \omega_q^{(j)2})} \quad [i = 1, 2, \dots, 9; \vartheta = 1, 2]. \quad (7)$$

Here,  $\omega_q^{(j,-TO\nu)}$  denote the modes obtained by eliminating the contribution of the  $\vartheta$  th TO mode of the high-k, and  $\phi_{q,\omega}^{TO\vartheta,i}$  denotes the contribution of the  $\vartheta$  th TO mode of the high-k in the  $i$  th coupled mode. To verify consistency of this process, we also checked the normalization condition  $\sum_i \phi_{q,\omega}^{TO\vartheta,i} = 1$ . The contribution of the two high-k TO phonons in different coupled modes are shown in Figs. 3(a) and 3(b). As seen in Fig. 3(a), the SO1 phonon contribution is small in plasmon mode as the phonon and plasmon energy are different. However, significant coupling to plasmon mode is observed for the SO2 phonon mode. An important point to mention here is that we have extracted the surface mode content from the TO phonons of the high-k only, as we

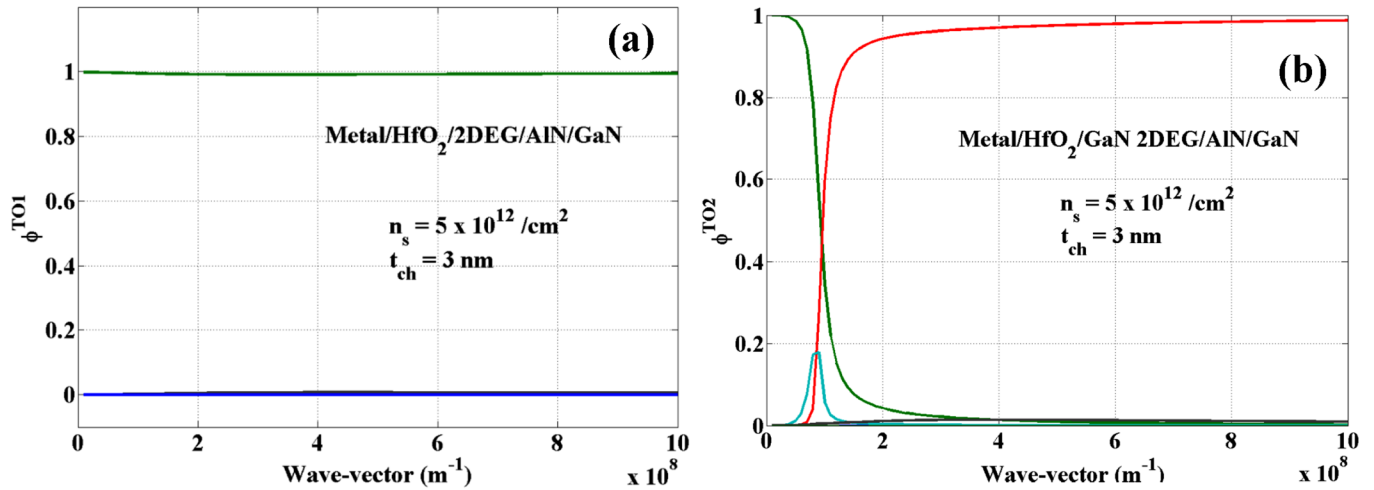


FIG. 3. (a) TO1 phonon content in different coupled surface modes; (b) TO2 phonon content in different coupled surface modes.

are interested in evaluating the effect of high- $k$  on the mobility in the 2-DEG. Both AlN and GaN TO modes also contribute to the coupled modes.

### C. Electron-surface mode interaction hamiltonian

From the secular equation set obtained by applying electrostatic boundary conditions on the screened phonon fields, we obtained the dispersion of the coupled modes. However, to obtain all the coefficients in the phonon field expression (Coefficients in Eq. (1) after screening), we need to consider one more equation. That is obtained by equating the semi classically obtained energy of the system due to the presence of the 2DEG in the phonon field with the ground state energy of a quantum harmonic oscillator<sup>25</sup>

$$\int \phi_{q,\omega_q}^{scr}(z) \rho_{q,\omega_q}^{scr}(z) dz = \frac{1}{2} \hbar \omega_q^j. \quad (8)$$

This integral on the left hand side of Eq. (8) is calculated numerically, and the coefficients of the screened phonon fields (Coefficients in Eq. (1) after screening) are extracted from there. We are interested only with  $c_{q,\omega}$  and  $d_{q,\omega}$  since the 2DEG exists only in the region  $0 \leq z < t_{ch}$ . The SO-phonon mode interaction Hamiltonian is given by

$$H_{q,\omega_q}^{int} = \frac{e}{\sqrt{\Omega}} (c_{q,\omega} \exp(qz) + d_{q,\omega} \exp(-qz)) \times [\exp(i\mathbf{q}\cdot\mathbf{r}) a_q^+ + \exp(-i\mathbf{q}\cdot\mathbf{r}) a_q], \quad (9)$$

with  $\Omega$  being the normalization area,  $\mathbf{q}$  is the two-dimensional phonon wave vector,  $\mathbf{r}$  is the two-dimensional position vector, and  $a_q^+$  ( $a_q$ ) is the phonon creation (annihilation) operator. Now, the coupling matrix between a single electron and the surface modes is calculated by

$$M_{q,\omega_q^j} = \langle \psi_{\mathbf{k}'}^* | H_{q,\omega_q^j}^{int} | \psi_{\mathbf{k}} \rangle, \quad (10)$$

where  $\psi_{\mathbf{k}}$  and  $\psi_{\mathbf{k}'}$  are single electron wavefunctions assuming a plane wave basis with an effective mass of 0.2 and  $\mathbf{k}$

and  $\mathbf{k}'$  are the two-dimensional electron wave vector before and after scattering.

The electron wave function can be determined using variational calculations.<sup>17,39</sup> However, the variational calculation has closed form analytical expressions only for cases when the normalized electric field ( $\tilde{F} = \frac{eFt_{ch}}{E_1^{(0)}}$ ,  $E_1^{(0)}$  is the unperturbed ground state energy and  $F$  is the electric field out of the 2DEG plane) is either much higher than 1 or much less than 1. But, we do have situations when  $\tilde{F}$  is in the vicinity of 1 (for  $t_{ch} \sim 3$  nm). Under such situations, the electron wavefunction and the ground state Eigen energy are calculated numerically solving the variational wave function.<sup>39</sup>

### III. IMPLEMENTATION OF SCATTERING BY RODE'S METHOD

Next, we discuss the implementation of the scattering process. The SO phonon scattering process in the transport of electrons cannot be implemented with reasonable accuracy under the relaxation time approximation (RTA) because it is valid only where the scattering mechanisms are elastic and isotropic, whereas SO phonon scattering is neither elastic nor isotropic. Hence, we follow another formalism, called Rode's method, that solves the electron distribution function iteratively and the method gives exact result as long as the in-plane electric field is low.<sup>40</sup> Here, we use it to estimate SO phonon limited electron mobility in GaN 2DEG which is a quasi 2D system. In the following, we briefly describe Rode's method.<sup>31</sup>

The master equation to solve electron distribution function under non-equilibrium condition is the well-known Boltzmann transport equation (BTE) which has the form

$$v \frac{\partial f}{\partial z} + \frac{eF_z}{\hbar} \frac{\partial f}{\partial k} = \sum_{\mathbf{k}'} \{ P(\mathbf{k}', \mathbf{k}) f(\mathbf{k}') [1-f(\mathbf{k})] - P(\mathbf{k}, \mathbf{k}') f(\mathbf{k}) [1-f(\mathbf{k}')] \}, \quad (11)$$

where  $f$  is the electron distribution function,  $v$  is the group velocity of electrons,  $F_z$  is the applied electric field in

z-direction (transport direction), and  $P(\mathbf{k}', \mathbf{k})$  and  $P(\mathbf{k}, \mathbf{k}')$  are the scattering rate between the states  $\mathbf{k}' \rightarrow \mathbf{k}$  and  $\mathbf{k} \rightarrow \mathbf{k}'$ , respectively. The two terms on the right hand side of Eq. (11) correspond to total in-scattering rate to state  $\mathbf{k}$  and total out-scattering rate from state  $\mathbf{k}$ , respectively. The scattering rate can be obtained from Fermi golden rule

$$P(\mathbf{k}, \mathbf{k}') = \frac{2\pi}{\hbar} |M_{\mathbf{q}, \omega_{\mathbf{q}}^i}|^2 \delta(\xi_{\mathbf{k}} - \xi_{\mathbf{k}'} \pm \hbar \omega_{\mathbf{q}}^i) \delta(\mathbf{k}', \mathbf{k} \pm \mathbf{q}), \quad (12)$$

where the (+ve) sign is for absorption of phonon and (−ve) sign is for emission of a phonon. The delta functions arise due to the conservation of energy and conservation of momentum during the scattering event. In Rode's method, the electron distribution function is expressed in terms of Legendre polynomials keeping only the first order term

$$f(\mathbf{k}) = f_0(k) + g(k) \cos \varphi. \quad (13)$$

Here, the equilibrium distribution function,  $f_0(k)$ , is taken according to Fermi-Dirac statistics.  $g(k)$  is the perturbation produced by the low electric field, and  $\varphi$  is the angle between the electric field  $F_z$  and the electron crystal momentum  $\mathbf{k}$ . Substituting this form of distribution in Eq. (11), we obtain

$$\begin{aligned} v \frac{\partial f_0}{\partial z'} + \frac{eF_z}{\hbar} \frac{\partial f_0}{\partial k} \\ = \int X g(k') \{P(\mathbf{k}', \mathbf{k}) [1 - f_0(\xi)] + P(\mathbf{k}, \mathbf{k}') f_0(\xi)\} d^2 \mathbf{k}' \\ - g(k) \int \{P(\mathbf{k}', \mathbf{k}) [1 - f_0(\xi)] + P(\mathbf{k}, \mathbf{k}') f_0(\xi')\} d^2 \mathbf{k}'. \end{aligned} \quad (14)$$

Here,  $X$  is the cosine of the angle between  $\mathbf{k}$  and  $\mathbf{k}'$ . The elastic scattering processes can be separated out, and the RTA scheme can be applied only on the elastic mechanisms, leaving the inelastic mechanisms intact. Doing so, Eq. (14) turns to

$$\begin{aligned} g(\mathbf{k}) \left( S_{\text{OUT}} + \frac{1}{\tau_m} \right) &= S_{\text{IN}}(g') - v \left( \frac{\partial f_0}{\partial z'} \right) - \left( \frac{eF_z}{\hbar} \right) \left( \frac{\partial f_0}{\partial k} \right), \\ S_{\text{OUT}} &= \int \{P(\mathbf{k}, \mathbf{k}') [1 - f_0(\xi')] \\ &\quad + P(\mathbf{k}', \mathbf{k}) f_0(\xi')\} d^2 \mathbf{k}', \\ S_{\text{IN}} &= \int X g(\mathbf{k}') \{P(\mathbf{k}', \mathbf{k}) [1 - f_0(\xi)] \\ &\quad + P(\mathbf{k}, \mathbf{k}') f_0(\xi)\} d^2 \mathbf{k}'. \end{aligned} \quad (15)$$

Here,  $1/\tau_m$  is the elastic scattering rate calculated using RTA.  $S_O$  and  $S_{IN}$  are the inelastic out- and in-scattering rates. Eq. (15) is a contraction mapping and can be solved iteratively with an initial  $g(k)$  given by RTA.

#### IV. $S_{\text{IN}}$ AND $S_{\text{OUT}}$ FOR 2DEG

First, we evaluate the inelastic in-scattering rate for SOP scattering. The scattering rate can be evaluated using Eq. (12). The product of  $\delta$ -functions can be combined to a single  $\delta$ -function<sup>41</sup>

$$\delta(\mathbf{k}, \mathbf{k} \pm \mathbf{q}) \delta(E' - E \mp \hbar \omega_{\mathbf{q}}^i) \rightarrow \frac{1}{\hbar v q} \delta\left(\pm \cos \theta + \frac{\hbar q}{2p} \mp \frac{\omega_{\mathbf{q}}^i}{v q}\right). \quad (16)$$

$$P(\mathbf{k}, \mathbf{k}') = \frac{2\pi}{\hbar} |M_{\mathbf{q}, \omega_{\mathbf{q}}^i}|^2 \delta\left(\pm \cos \theta + \frac{\hbar q}{2p} \mp \frac{\omega_{\mathbf{q}}^i}{v q}\right), \quad (17)$$

where  $\theta$  is the angle between  $\mathbf{k}$  and  $\mathbf{q}$ , and  $\mathbf{q}$ ,  $\mathbf{v}$ , and  $\mathbf{p}$  are phonon wave vector, the electron velocity, and momentum, respectively. The relationship between the electron wave vectors and phonon wave vector is shown in inset of Fig. 4(b), from which we get

$$\cos \alpha = \frac{|\mathbf{k}|}{|\mathbf{k} + \mathbf{q}|} \pm \frac{|\mathbf{q}|}{|\mathbf{k} + \mathbf{q}|} \cos \theta. \quad (18)$$

Due to the conservation of momentum, we can convert the integral over  $\mathbf{k}'$  to integral over  $\mathbf{q}$  ( $\sum_{\mathbf{q}}(\cdot) \rightarrow \frac{1}{4\pi^2} \int dq d\theta$ ). Using the Eq. (15)–(18), we get Eq. (19a) for the in-scattering rate with  $N_{\omega_{\mathbf{q}}^i}$  being the Bose-Einstein phonon occupation number at temperature  $T$ . The  $\delta$ -function integral results to Eqs. (20a)–(20b). The delta function also puts limit on the allowed phonon wave vectors. Similar expression can be found for the out-scattering rate (Eq. (19b)).

The calculated out-scattering ( $S_{\text{OUT}}$ ) and in-scattering ( $S_{\text{IN}}$ ) rates are plotted in Figs. 4(a) and 4(b), respectively, as a function of the electron energy (for HfO<sub>2</sub> dielectric on 3 nm GaN channel with a 2DEG density of  $5 \times 10^{12} \text{ cm}^{-2}$ ). The GaN device structure and doping density are given in Fig. 1. The sharp kinks shown in the plots represent the onset of phonon emission, while the tiny jitters arise from numerical gridding of the  $q$  space. The energy independent elastic scattering rate ( $1/\tau_m = 1 \times 10^{11} \text{ s}^{-1}$ ) is chosen to be low to clearly reveal the impact of SO phonon scattering on mobility

$$\begin{aligned} S_{\text{IN}}(\mathbf{k}) &= \frac{1}{2\pi \hbar^2 v} \sum_i \left[ \int_{\mathbf{q}} g'(|\mathbf{k} \pm \mathbf{q}|) \left( N_{\omega_{\mathbf{q}}^i} + \frac{1}{2} \mp \frac{1}{2} \right) \right. \\ &\quad \times \left\{ |M_{\mathbf{q}, \omega_{\mathbf{q}}^i}|^2 [f_0(\xi)] \right\} \cdot \left\{ \int \left( \frac{\mathbf{k}}{|\mathbf{k} \pm \mathbf{q}|} \pm \frac{\mathbf{q}}{|\mathbf{k} \pm \mathbf{q}|} \cos \theta \right) \right. \\ &\quad \times \delta \left( \pm \cos \theta + \frac{q}{2k} \mp \frac{\omega_{\mathbf{q}}^i}{v q} \right) d\theta \left. \right\} \cdot d\mathbf{q} \\ &\quad + \frac{m}{2\pi \hbar^3} \int_{\mathbf{q}'} \left[ g'(|\mathbf{k} \mp \mathbf{q}|) \frac{1}{4\pi^2} \left( N_{\omega_{\mathbf{q}}^i} + \frac{1}{2} \mp \frac{1}{2} \right) \right. \\ &\quad \times \left\{ |M_{\mathbf{q}, \omega_{\mathbf{q}}^i}|^2 [1 - f_0(\xi)] \right\} \frac{1}{|\mathbf{k} \mp \mathbf{q}|} \\ &\quad \times \left\{ \int \left( \frac{|\mathbf{k} \mp \mathbf{q}|}{k} \pm \frac{q}{k} \cos \theta \right) \right. \\ &\quad \times \delta \left( \pm \cos \theta + \frac{q}{2|\mathbf{k} \mp \mathbf{q}|} \mp \frac{m \omega_{\mathbf{q}}^i}{\hbar |\mathbf{k} \mp \mathbf{q}| q} \right) \cdot d\theta \left. \right\} \cdot d\mathbf{q}, \end{aligned} \quad (19a)$$

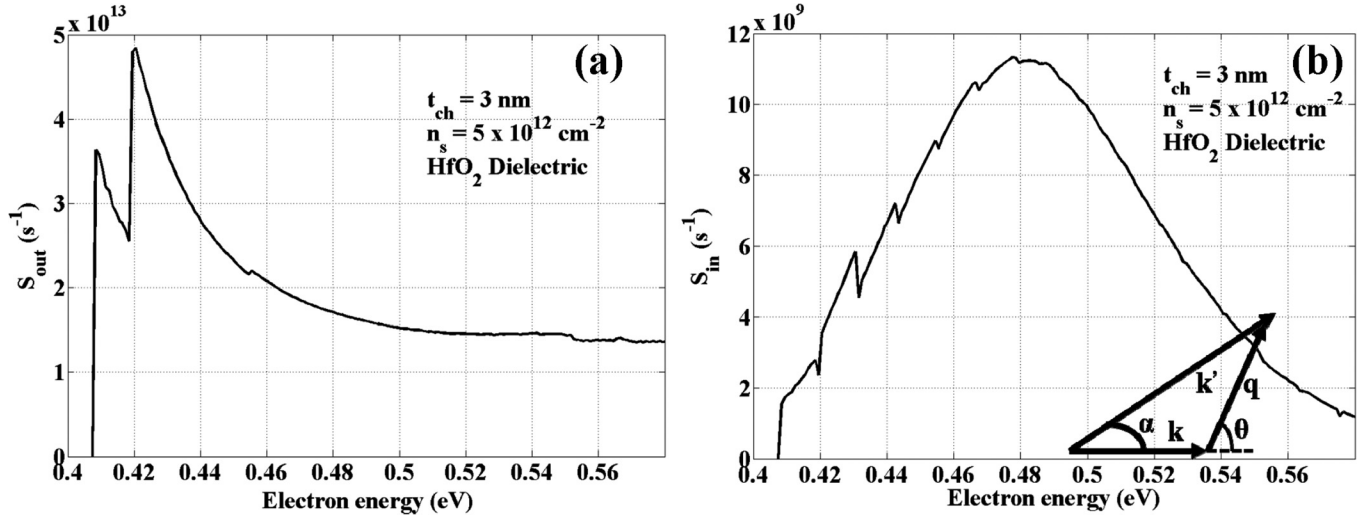


FIG. 4. (a) Out-scattering rate by GaN 2DEG. (b) In-scattering rate by GaN 2DEG (inset) schematic of momentum conservation during interaction of an electron with surface mode.

$$\begin{aligned}
 S_{\text{OUT}}(\mathbf{k}) = & \sum_i \left[ \frac{1}{2\pi\hbar^2 v} \int_q \left( N_{\omega_q^i} + \frac{1}{2} \mp \frac{1}{2} \right) \right. \\
 & \times \left\{ |M_{q,\omega_q^i}|^2 \left[ 1 - f_0(\xi \pm \hbar\omega_q^i) \right] \right\} \\
 & \times \left\{ \int \delta \left( \pm \cos \theta + \frac{q}{2k} \mp \frac{\omega_q^i}{vq} \right) \cdot d\theta \right\} \cdot dq \Bigg] \\
 & + \left[ \frac{m}{2\pi\hbar^3} \int_{q'} \left( N_{\omega_{q'}^i} + \frac{1}{2} \mp \frac{1}{2} \right) \right. \\
 & \times \left\{ |M_{q,\omega_{q'}^i}|^2 \left[ f_0(\xi \pm \hbar\omega_{q'}^i) \right] \right\} \frac{1}{|\mathbf{k} \mp \mathbf{q}|} \\
 & \times \left\{ \int \delta \left( \pm \cos \theta + \frac{q}{2|\mathbf{k} \mp \mathbf{q}|} \mp \frac{m\omega_{q'}^i}{\hbar|\mathbf{k} \mp \mathbf{q}|q} \right) d\theta \right\} dq \Bigg], \quad (19b)
 \end{aligned}$$

$$\int \delta \left( \pm \cos \theta + \frac{q}{2k} \mp \frac{\omega_q^i}{vq} \right) \cdot d\theta = \frac{1}{\left( \sqrt{1 - \left( \frac{q}{2k} \mp \frac{\omega_q^i}{vq} \right)^2} \right)}, \quad (20a)$$

$$\int \cos \theta \delta \left( \pm \cos \theta + \frac{q}{2k} \mp \frac{\omega_q^i}{vq} \right) \cdot d\theta = \frac{\frac{q}{2k} \mp \frac{\omega_q^i}{vq}}{\left( \sqrt{1 - \left( \frac{q}{2k} \mp \frac{\omega_q^i}{vq} \right)^2} \right)}. \quad (20b)$$

## V. SCREENING OF THE COUPLED MODES: EFFECT OF LANDAU DAMPING

Plasmons cease to respond in the single particle excitation (SPE) regime.<sup>36,42</sup> We take this into account approximately by turning off the plasmon contribution from the GaN dielectric response in the SPE regime (Landau damping). The effect of doing so has implication on the dependence of mobility on the

2DEG density. We discuss this issue here. Fig. 6(a) shows the dispersion of the three branches of the plasmon-coupled surface modes originating from the TO modes of HfO<sub>2</sub> under 2DEG densities of  $5 \times 10^{12} \text{ cm}^{-2}$ . It can be seen that the plasmon couples well with one of the surface modes in the long-wavelength limit. Initially the phonon like mode is above the plasmon like mode, producing anti-screening of the former while the converse is true as the wave-vector increases. This phenomenon can be observed in the effective screening plot shown in Fig. 6(b), where the screening drops to a negligible value (the plot shows reciprocal of screening and hence peaks up) in the vicinity of  $q = 1 \times 10^8 \text{ m}^{-1}$ . However, beyond that point, the plasmons undergo Landau damping killing the anti-screening effect and the only screening contribution comes from the bulk TO mode of GaN. For higher 2DEG densities, Landau damping occurs much prior compared to the case for lower 2DEG density because of a steeper intraband SPE boundary. Hence, the sharp anti-screening effect is not observed, and the surface modes are better screened compared to a lower 2DEG density case.

## VI. RESULTS AND DISCUSSIONS

Fig. 5 shows the convergence of the first order harmonic (Eq. (13)) in the distribution function with HfO<sub>2</sub> as the dielectric. Once the iteration converges, the 2DEG mobility can readily be calculated by

$$\mu_n = \frac{m^*}{2\pi\hbar^2 F_z n_s} \int_0^\infty g_{\text{steady}}(E) v(E) dE. \quad (21)$$

Here,  $g_{\text{steady}}(E)$  is the first order harmonic in the electron distribution after Rode's iteration has converged, and  $v(E)$  is the magnitude of the in-plane velocity of the 2DEG. The mobility expressed in Eq. (21) is extracted from the current density calculated by  $J = \frac{e}{A} \sum_{\mathbf{k}} v(\mathbf{k}) f(\mathbf{k})$ , and the derivation of it is shown in Appendix B. As the elastic scattering rate has been artificially assumed to be low, the calculated mobility is the SO phonon limited mobility. The bulk LO phonon limited mobility is the dominant scattering that limits mobility in GaN

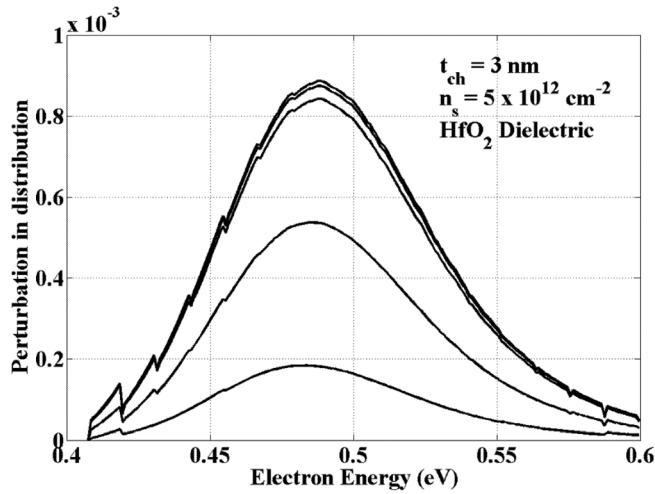


FIG. 5. The convergence of the first order harmonic in electron distribution by Rode's iteration.

2DEGs (order of  $2000 \text{ cm}^2/\text{V.s}$ ).<sup>2</sup> The mobility degradation due to SO phonons would take place if the SO limited mobility is comparable to bulk polar optical phonon limited mobility.

The calculation methods described above are carried out for the structure shown in Fig. 1 for different dielectrics, different GaN channel thickness, and different 2DEG densities. In practice, the 2DEG density in the structure can be changed by the application of a gate electric field. Figs. 7(a) and 7(b) show the variation of mobility with 2DEG density for GaN channel thicknesses of 3 nm and 5 nm, respectively. The elastic scattering limited mobility is calculated to be  $88\,000 \text{ cm}^2/\text{V.s}$ . In the following, we discuss the SO phonon mediated electron mobility degradation for each dielectric.

### A. HfO<sub>2</sub> and ZrO<sub>2</sub> as high- $\kappa$

As seen in Figs. 7(a)–7(b), the SO limited mobility due to HfO<sub>2</sub> and ZrO<sub>2</sub> are similar due to the similar values of the corresponding TO phonon energies. As the channel thickness is reduced, the electron wave function gets closer to the high- $k$  gate dielectric and the overlap with the exponentially decaying SO mode increases, which results in increased

scattering and lower mobility. At larger channel thickness ( $\geq 5 \text{ nm}$ ), the overlap is small and the SO limited mobility is  $>10\,000$ , which is 5 times higher than the bulk limited mobility. Hence, no degradation in mobility due to SO phonons is expected for  $t_{\text{ch}} \geq 5 \text{ nm}$ .

However, for extremely scaled channel thickness ( $<5 \text{ nm}$ ), SO phonon scattering is found to be quite pronounced degrading the mobility below  $5000 \text{ cm}^2/\text{V.s}$  (Figs. 7(a)–7(b)) for both HfO<sub>2</sub> and ZrO<sub>2</sub>. From Figs. 7(a) and 7(b), we see that the mobility increases with 2DEG density. As we increase the 2DEG density, the electric field due to heterojunction at the GaN/AlN interface decreases, which should spread the electron cloud more towards the high- $k$  interface increasing overlap with SO modes, which would decrease mobility. However, as the 2DEG density is increased, there is enhanced screening of the surface modes, which weakens their coupling with the 2DEG, and hence, mobility improves.

### B. Al<sub>2</sub>O<sub>3</sub> as high- $\kappa$

The plasmon coupling of SO modes for Al<sub>2</sub>O<sub>3</sub> is significant because of comparable energies in the range of phonon wavevectors ( $q$ ) of interest. This increases the energy of the SO modes, which decreases the phonon occupancy ( $N_q$ ). Hence, the SO limited mobility is higher due to the higher SO phonon energies (Fig. 8(a)). The 3 nm quantum well mobility drops to around  $2000 \text{ cm}^2/\text{V.s}$  for low 2DEG densities, hence will degrade the total mobility at this channel thickness. However, the mobility rapidly increases at higher 2DEG densities to large values. The non-monotonicity of mobility with increasing 2DEG density is a result of an interplay between improved screening and higher overlap of the decaying surface modes and the electron wavefunction. The slight decline in mobility at moderate 2DEG density ( $n_s$ ) occurs because at that range of  $n_s$ , the screening of the mode arising from the lower TO energy is saturated while that from the higher TO energy begins.

### C. SiN as high- $\kappa$

As noted above, the SO scattering for 3 nm GaN channel devices will degrade the mobility significantly for Al<sub>2</sub>O<sub>3</sub>, HfO<sub>2</sub>, and ZrO<sub>2</sub> dielectrics. SiN gate dielectric has been

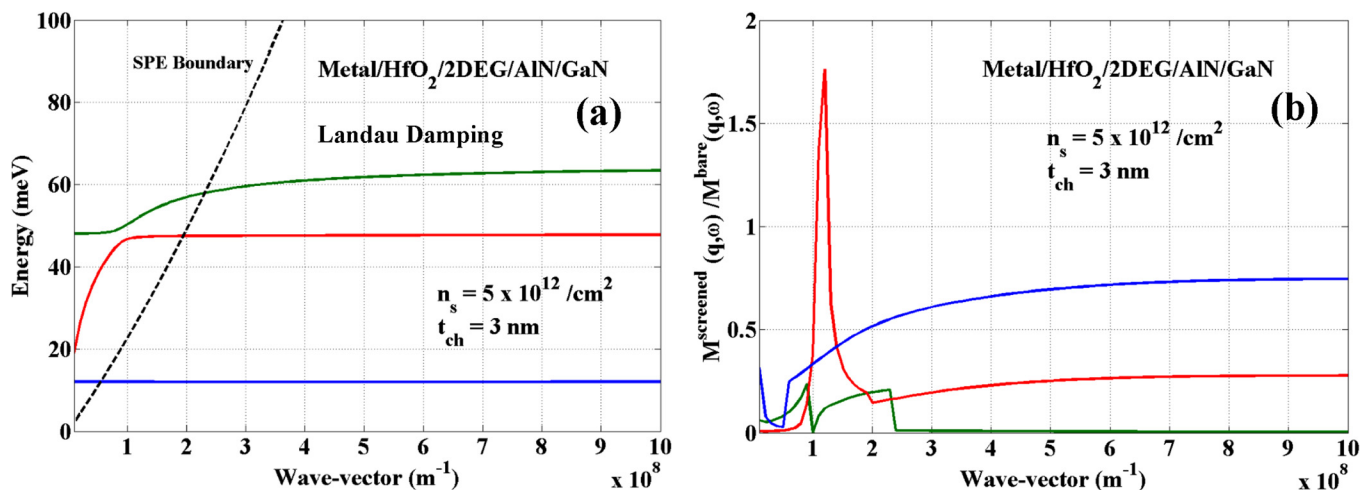


FIG. 6. (a) Relative separation of the main three surface modes (the high- $k$  TO modes coupled with GaN plasmon) that affect mobility and the single particle excitation regime boundary. (b) Screening effect on those three modes with Landau damping being taken care of by turning off plasmon response in the SPE region.

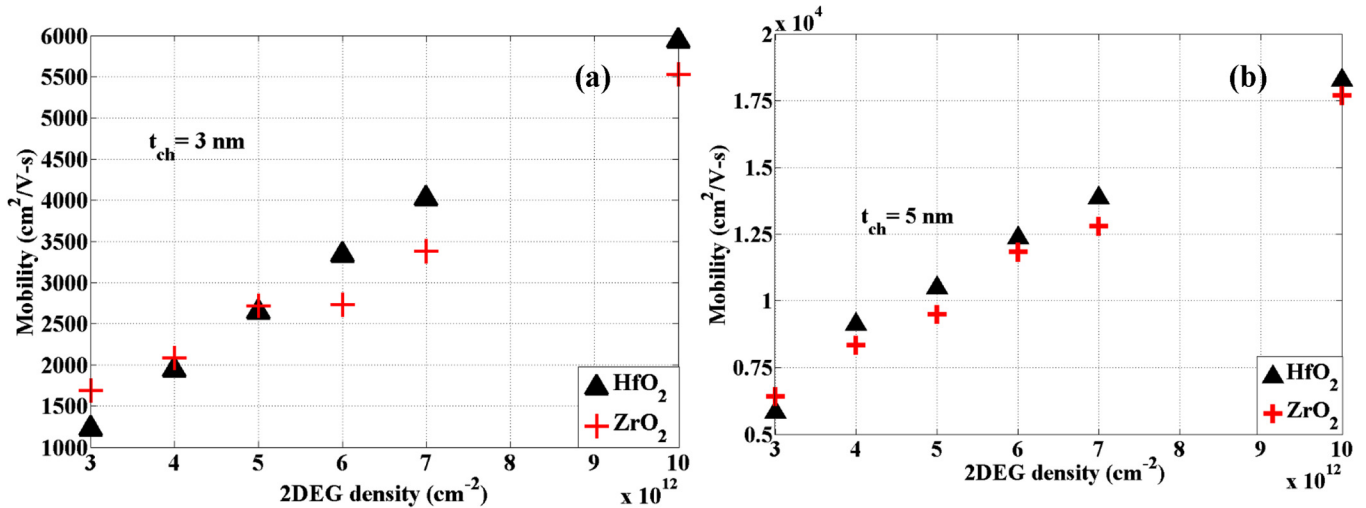


FIG. 7. (a) Dependence of surface mode scattering mediated mobility on density of 2DEG for a quantum well thickness ( $t_{ch}$ ) of 3 nm and with HfO<sub>2</sub> and ZrO<sub>2</sub>; (b) similar plots for  $t_{ch} = 5$  nm.

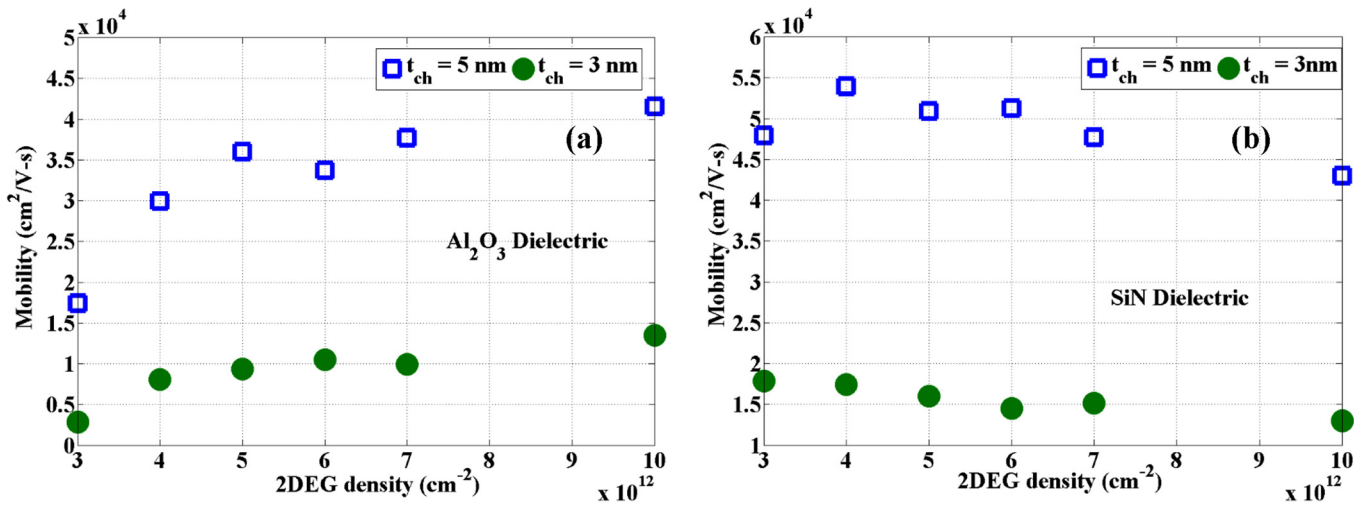


FIG. 8. (a) Dependence of surface mode scattering mediated mobility on density of 2DEG for Al<sub>2</sub>O<sub>3</sub> for two different channel thickness; (b) similar plots for SiN.

widely used in N-polar GaN devices. It has lower dielectric constant, however the phonon energy is very high ( $\omega_{TO} = 103$  meV). Here, we calculate the SO limited mobility for SiN gate dielectric. Fig. 8(b) shows the dependence of mobility on 2DEG density when SiN is used as a gate dielectric. It can be seen that SiN is definitely superior in terms of SO limited mobility to other dielectrics. The reason is higher SO phonon energy that results in very low phonon occupancy factors resulting in a low scattering rate. The slightly decreasing trend of mobility with 2DEG is a result of increasing electron surface mode coupling due to reduced electric field at the GaN/AlN junction. Screening does not have much role at low 2DEG densities in this case because the SO phonon energy is high enough that neither the GaN plasmon nor the GaN TO mode could screen it. However, as seen from Fig. 8(b), at high 2DEG densities ( $>7 \times 10^{12}$  cm<sup>-2</sup>), screening slightly improves the mobility. Overall, we can say, that screening has negligible effect in case of SiN, and the mobility is controlled by the overlap of the surface mode and the electron wave function.

## VII. CONCLUSION

Surface optical (SO) phonon scattering is explored in N-polar GaN quantum well systems. Using Rode's iterative method helped to relax the RTA which is not a good approximation to deal with inelastic scatterings. Coupling of the surface modes with GaN plasmon is explored and screening properties are investigated. In summary, we have calculated the SO phonon scattering rates of Al<sub>2</sub>O<sub>3</sub>, ZrO<sub>2</sub>, HfO<sub>2</sub>, and SiN dielectrics on GaN quantum well channels. The SO mobility at 5 nm thickness is found to be  $>4 \times$  higher than the experimentally reported mobilities.<sup>19,20</sup> However, the SO limited mobility becomes a limiting factor at 3 nm GaN channel thickness and will severely degrade the 2DEG mobility for HfO<sub>2</sub> and ZrO<sub>2</sub> dielectrics, and also for Al<sub>2</sub>O<sub>3</sub> at low 2-DEG densities ( $<4 \times 10^{12}$  cm<sup>-2</sup>). For Al<sub>2</sub>O<sub>3</sub>, the SO limited 2-DEG mobility is  $>5 \times$  the bulk phonon mobility at higher 2DEG densities ( $\geq 4 \times 10^{12}$  cm<sup>-2</sup>). The SO limited scattering for SiN dielectric is found to be negligible due to its high TO energy (see Table I), giving SO limited mobilities  $>15000$  cm<sup>2</sup>/V.s. By careful design of composite gate stack

that incorporates interfacial SiN and high-k dielectrics such as HfO<sub>2</sub> and ZrO<sub>2</sub>, both high mobility and low EOT can be obtained in ultra-thin GaN (<5 nm) channels.

## APPENDIX A: GREEN'S FUNCTION TO IMPLEMENT SCREENING IN HIGH-K/GAN/ALN/GAN STRUCTURE

In this Appendix, we discuss the form of Green's function we showed in Sec. II A.

$$G_q(z, z') = -\frac{1}{2q\varepsilon_{\text{GaN}}^0} \begin{cases} \alpha_q [\exp(q(z-z')) + \exp(-q(z+z'+2t_{\text{ox}}))]q & -t_{\text{ox}} \leq z < 0 \\ \beta_q \exp(-q|z-z'|) + \gamma_q \exp(-q(z+z')) + \eta_q \exp(q(z+z')) & 0 \leq z < t_{\text{ch}} \\ \kappa_q \exp(-q(z-z')) + \lambda_q \exp(q(z+z')) & t_{\text{ch}} \leq z \leq t_{\text{ch}} + t_{\text{AlN}} \\ \varsigma_q \exp(-q(z-z')) & z \geq t_{\text{ch}} + t_{\text{AlN}} \end{cases}$$

The Green's function  $G_q(z, z')$  accounts for the screening effect by a charge present at position  $z'$  on the potential at position  $z$  due to the surface modes. Because of the confinement of the 2DEG,  $z'$  can be only between 0 and  $t_{\text{ch}}$ . This explains the presence of the absolute sign in the argument of the first decaying term (Eq. (4)) when  $z$  is between 0 and  $t_{\text{ch}}$ . The pre-factor contains the term  $\varepsilon_{\text{GaN}}^0$  which comes from the background lattice contribution of GaN. The Dirichlet and Neumann boundary conditions for the Green's function are listed below

$$\begin{aligned} G_q(z=0^+, z') &= G_q(z=0^+, z'); \quad \frac{\varepsilon_{\text{ox}}^\infty dG_q(z=0^-, z')}{dz} = \frac{\varepsilon_{\text{GaN}}^0 dG_q(z=0^+, z')}{dz}; \\ G_q(z=t_{\text{ch}}^-, z') &= G_q(z=t_{\text{ch}}^+, z'); \quad \frac{\varepsilon_{\text{GaN}}^0 dG_q(z=t_{\text{ch}}^-, z')}{dz} = \frac{\varepsilon_{\text{AlN}}^0 dG_q(z=t_{\text{ch}}^+, z')}{dz} \quad (\text{A1}) \\ G_q(z=(t_{\text{ch}}+t_{\text{AlN}})^-, z') &= G_q(z=(t_{\text{ch}}+t_{\text{AlN}})^+, z'); \\ \frac{\varepsilon_{\text{AlN}}^0 dG_q(z=(t_{\text{ch}}+t_{\text{AlN}})^-, z')}{dz} &= \frac{\varepsilon_{\text{GaN}}^0 dG_q(z=(t_{\text{ch}}+t_{\text{AlN}})^+, z')}{dz}. \end{aligned}$$

These conditions are accompanied by one more condition which signifies the presence of the delta function at the  $z = z'$  point

$$\frac{dG_q(z=z'^-, z')}{dz} - \frac{dG_q(z=z'^+, z')}{dz} = -1. \quad (\text{A2})$$

The six equations in (A1) and Eq. (A2) can together be used to extract the coefficients.

## APPENDIX B: MOBILITY CALCULATION FOR 2DEG

In this Appendix, we show the derivation of the mobility expression shown in Eq. (21). In the following, we take  $\mathbf{v}_x(\mathbf{k})$  to be the velocity of an electron in the direction of parallel electric field and  $\varphi$  to be the angle between the velocity of an electron and the parallel electric field. The current density can be written as

$$\begin{aligned} J_x &= -\frac{e}{A} \sum_{\mathbf{k}} \mathbf{v}_x(\mathbf{k}) f(k) = -\frac{e}{A} \sum_{\mathbf{k}} \mathbf{v}_x(\mathbf{k}) g(k) \cos \varphi \quad [\text{Contribution from the equilibrium distribution function is zero}] \\ &= -\frac{e}{A} \sum_{\mathbf{k}} \mathbf{v}(\mathbf{k}) g(k) \cos^2 \varphi = -\frac{e}{A} \cdot \frac{A}{2\pi^2} \int k v(k) g(k) dk \int \cos^2 \varphi d\varphi \quad [\text{Spin degeneracy is taken into account}] \\ &= -\frac{e}{2\pi} \int k v(k) g(k) dk. \end{aligned} \quad (\text{B1})$$

From the definition of mobility ( $\mu$ ), we can write

$$J_x = -\mu n_s F_x. \quad (\text{B2})$$

Here,  $n_s$  is the density of the 2DEG, and  $F_x$  is the parallel electric field. Hence, mobility can be written as

$$\mu_n = \frac{m^*}{2\pi \hbar^2 F_x n_s} \int_0^\infty g(E) v(E) dE. \quad (\text{B3})$$

This is a mobility expression for a 2DEG under a parallel electric field low enough to ignore the higher order spherical harmonics of the distribution function. This expression can be used to calculate mobility limited by other scattering mechanisms as well (like Coulomb scattering).

<sup>1</sup>U. K. Mishra, P. Parikh, and Y.-F. Wu, *Proc. IEEE* **90**(6), 1022–1031 (2002).

<sup>2</sup>Y. Cao, H. Xing, and D. Jena, *Appl. Phys. Lett.* **97**(22), 222116 (2010).

- <sup>3</sup>E. Ahmadi, H. Chalabi, S. W. Kaun, R. Shivaraman, J. S. Speck, and U. K. Mishra, *J. Appl. Phys.* **116**(13), 133702 (2014).
- <sup>4</sup>T.-H. Hung, M. Esposito, and S. Rajan, *Appl. Phys. Lett.* **99**(16), 162104 (2011).
- <sup>5</sup>D. Ji, Y. Lu, B. Liu, G. Jin, G. Liu, Q. Zhu, and Z. Wang, *J. Appl. Phys.* **112**(2), 024515 (2012).
- <sup>6</sup>D. Ji, B. Liu, Y. Lu, G. Liu, Q. Zhu, and Z. Wang, *Appl. Phys. Lett.* **100**(13), 132105 (2012).
- <sup>7</sup>D. F. Brown, S. Rajan, S. Keller, Y.-H. Hsieh, S. P. DenBaars, and U. K. Mishra, *Appl. Phys. Lett.* **93**(4), 042104 (2008).
- <sup>8</sup>D. S. Lee, L. Bin, M. Azize, G. Xiang, G. Shipping, D. Kopp, P. Fay, and T. Palacios, *Tech. Dig. – Int. Electron Devices Meet.* **2011**, 19.12.11–19.12.14.
- <sup>9</sup>B. Lu, E. Matioli, and T. Palacios, *IEEE Electron Device Lett.* **33**(3), 360–362 (2012).
- <sup>10</sup>K. Shinohara, D. Regan, A. Corrion, D. Brown, I. Alvarado-Rodriguez, M. Cunningham, C. Butler, A. Schmitz, S. Kim, B. Holden, D. Chang, V. Lee, and P. M. Asbeck, in *IEEE Compound Semiconductor Integrated Circuit Symposium (CSICS), 2012* (IEEE, 2012), pp. 1–4.
- <sup>11</sup>Y. Yue, Z. Hu, J. Guo, B. Sensale-Rodriguez, G. Li, R. Wang, F. Faria, T. Fang, B. Song, X. Gao, S. Guo, T. Kosel, G. Snider, P. Fay, D. Jena, and H. Xing, *IEEE Electron Device Lett.* **33**(7), 988–990 (2012).
- <sup>12</sup>S. Rajan, A. Chini, M. H. Wong, J. S. Speck, and U. K. Mishra, *J. Appl. Phys.* **102**(4), 044501–044506 (2007).
- <sup>13</sup>Nidhi, S. Dasgupta, D. F. Brown, S. Keller, J. S. Speck, and U. K. Mishra, *Tech. Dig. - Int. Electron Devices Meet.* **2009**, pp. 1–3.
- <sup>14</sup>U. Singiseti, M. H. Wong, J. S. Speck, and U. K. Mishra, *IEEE Electron Device Lett.* **33**(1), 26–28 (2012).
- <sup>15</sup>D. Denninghoff, J. Lu, M. Laurent, E. Ahmadi, S. Keller, and U. K. Mishra, in *70th Annual Device Research Conference (DRC), University Park, Pennsylvania, 18–20 June, 2012* (2012), pp. 151–152.
- <sup>16</sup>Nidhi, S. Dasgupta, J. Lu, J. S. Speck, and U. K. Mishra, *IEEE Electron Device Lett.* **33**(7), 961–963 (2012).
- <sup>17</sup>U. Singiseti, M. H. Wong, and U. K. Mishra, *Appl. Phys. Lett.* **101**(1), 012101–012104 (2012).
- <sup>18</sup>N. Nidhi, O. Bierwagen, S. Dasgupta, D. F. Brown, S. Keller, J. S. Speck, and U. K. Mishra, in *2010 Electronic Materials Conference (EMC), Norte Dame, Indiana 23–25 June, 2010* (2010).
- <sup>19</sup>D. Denninghoff, J. Lu, E. Ahmadi, S. Keller, and U. K. Mishra, in *39th International Symposium on Compound Semiconductors* (Santa Barbara, 2012).
- <sup>20</sup>J. Lu, M. Laurent, R. Chung, S. Lal, A. Szein, S. Keller, S. P. DenBaars, and U. K. Mishra, in *2012 Electronic Materials Conference (EMC)* (2012).
- <sup>21</sup>J. Lu, D. Denninghoff, S. Keller, S. P. DenBaars, and U. K. Mishra, in *International Workshop on Nitride Semiconductors 2012 (IWN2012)* (Sapporo, Japan, 2012).
- <sup>22</sup>J. Lu *et al.*, *Appl. Phys. Lett.* **104**(9), 092107 (2014).
- <sup>23</sup>K. Hess and P. Vogl, *Solid State Commun.* **30**(12), 797–799 (1979).
- <sup>24</sup>B. T. Moore and D. K. Ferry, *J. Appl. Phys.* **51**(5), 2603–2605 (1980).
- <sup>25</sup>M. V. Fischetti, D. A. Neumayer, and E. A. Cartier, *J. Appl. Phys.* **90**(9), 4587–4608 (2001).
- <sup>26</sup>T. P. O'Regan, M. V. Fischetti, B. Soree, S. Jin, W. Magnus, and M. Meuris, *J. Appl. Phys.* **108**(10), 103705–103711 (2010).
- <sup>27</sup>A. Konar, T. Fang, and D. Jena, *Phys. Rev. B* **82**(11), 115452 (2010).
- <sup>28</sup>A. Y. Serov, Z. Y. Ong, M. V. Fischetti, and E. Pop, "Theoretical analysis of high-field transport in graphene on a substrate," *J. Appl. Phys.* **116**(3), 034507 (2014).
- <sup>29</sup>S. Fratini and F. Guinea, *Phys. Rev. B* **77**(19), 195415 (2008).
- <sup>30</sup>I.-T. Lin and J.-M. Liu, *IEEE J. Sel. Top. Quantum Electron.* **20**(1), 8400108 (2014).
- <sup>31</sup>R. L. Rode, "Low-field electron transport," *Semicond. Semimet.* **10**, 1–89 (1975).
- <sup>32</sup>A. T. Ramu, L. E. Cassels, N. H. Hackman, H. Lu, J. M. Zide, and J. E. Bowers, *J. Appl. Phys.* **107**(8), 083707 (2010).
- <sup>33</sup>S. Q. Wang and G. D. Mahan, *Phys. Rev. B* **6**(12), 4517–4524 (1972).
- <sup>34</sup>P. Y. Yu and M. Cardona, in *Fundamentals of Semiconductors: Physics and Materials Properties* (Springer, Berlin Heidelberg, 2010), pp. 502–511.
- <sup>35</sup>D. V. Tsu, G. Lucovsky, and M. J. Mantini, *Phys. Rev. B* **33**(10), 7069–7076 (1986).
- <sup>36</sup>Z.-Y. Ong and M. V. Fischetti, "Theory of interfacial plasmon-phonon scattering in supported graphene," *Phys. Rev. B* **86**(16), 165422 (2012).
- <sup>37</sup>F. Stern, "Polarizability of a two-dimensional electron gas," *Phys. Rev. Lett.* **18**(14), 546 (1967).
- <sup>38</sup>O. Debieu, R. P. Nalini, J. Cardin, X. Portier, J. Perriere, and F. Gourbilleau, *Nanoscale Res. Lett.* **8**(1), 31 (2013).
- <sup>39</sup>D. Ahn and S. L. Chuang, *Appl. Phys. Lett.* **49**(21), 1450–1452 (1986).
- <sup>40</sup>D. K. Ferry, *Semiconductors* (IOP Publishing, 2013).
- <sup>41</sup>M. Lundstrom, in *Fundamentals of Carrier Transport* (Cambridge University Press, 2000), pp. 54–114.
- <sup>42</sup>B. K. Ridley, *Quantum Processes in Semiconductors* (Oxford University Press, 1993).